

Master's Thesis

# Commissioning and Characterization of Two Undulators at the MAX IV 3 GeV Storage Ring

Sara Mikaelsson  
In cooperation with  
MAX IV Laboratory



# Commissioning and Characterization of Two Undulators at the MAX IV 3 GeV Storage Ring

Master's Thesis

By

Sara Mikaelsson  
sara.mikaelsson@gmail.com

Department of Electrical and Information Technology  
Faculty of Engineering, LTH, Lund University  
SE-221 00 Lund, Sweden

Supervisor: Anders Karlsson  
Assistant Supervisors: Francesca Curbis & Hamed Tarawneh

September 13, 2016



LUND UNIVERSITY



Printed in Sweden  
E-huset, Lund, 2016

---

# Abstract

---

Insertion devices have several undesirable effects on the beam dynamics of a synchrotron storage ring, and these must be compensated for in order to ensure long term stable operation. This master's thesis concerns the two first insertion devices at the MAX IV facility, two in-vacuum undulators for the BioMAX and NanoMAX beamlines. The report presents the work done to neutralize closed-orbit distortions caused by the undulators using a feed-forward scheme, as well as investigations into effects on the optics, and non-linear effects on lifetime and beam size. An algorithm was developed which was able to automatically find feed-forward tables which reduced the closed-orbit distortions to noise level. This algorithm was adapted to be usable for future insertion devices at MAX IV. The tune shift and beta-beat was determined to be negligible and no compensation scheme was implemented. Beam displacement measurements were attempted and found to have insufficient range, thus highlighting the need for other methods to investigate non-linear effects in the future.

---

# Acknowledgements

---

I would like to thank my supervisors: Anders Karlsson for his cheerful encouragement, Fransesca Curbis for her support, and finally Hamed Tarawneh for his patience, trust and guidance. Thank you for making this graduation project possible!

A huge thanks to my partner, William Larsson, who has put up with me during this time and helped me with all things not academical.

Finally, thank you to the people of MAX IV; PhD students, lecturers and staff, for letting me do my master's thesis in such a exiting and dynamic place. Thanks for the help offered in the control room, the encouragement and the wonderful insight into the operation of a large scale research facility.

---

# Popular Science Summary

---

## Compensation of Insertion Device Effects at the MAX IV Laboratory

*In the public mind, accelerators are tools of particle physicists; huge machines which collide particles in the hope of uncovering the fundamental nature of matter. A more common type of accelerator is the synchrotron light-source, where the particles are of less interest than the light they emit. The devices that produce this light, however, cause disturbances which must be neutralized.*

MAX IV, the new state-of-the-art laboratory Lund, will open the door to many new exciting experiments in a wide variety of scientific fields. MAX IV is a synchrotron, an electron accelerator built for the purpose of producing high intensity, high energy radiation, primarily in the form of X-rays. The first users will be from the fields of life science and solid state physics, using the first two beamlines installed; the NanoMAX and BioMAX. These experiments will be carried out involving, for example, the structure of proteins and imaging of objects on the atomic scale. The X-rays which are used for these experiments are come from two identical so-called insertion devices.

While these insertion devices are essential for the high quality X-rays the experiments demand, they also disturb the equilibrium of the electrons travelling around the large 528 m circumference storage ring. The electrons in the ring travel at a speed incredibly close to the speed of light, and are steered around the ring by magnets. Every time the electrons are deflected by a magnet, they emit light. The insertion devices are made up by long arrays of permanent magnets generating magnetic fields with alternating direction. Through the device, the electrons are guided into a slalom path of sorts; they undulate, or wiggle. Depending on the strength of the devices, they are indeed called either undulators or wigglers. One notable effect of the wiggling path is that the orbit of the electrons around the ring is disturbed.

The undulators for the BioMAX and NanoMAX beamlines are relatively weak, but these disturbances still cannot be ignored. Around twenty devices will be installed in the ring, and if the orbit is not corrected, the cumulative effect of the devices will eventually cause the beam to hit the wall of the vacuum pipe which contains it. This is also true for other, more complicated, disturbances caused by the undulators.

The correction of the orbit is done by two so called corrector magnets, which can “kick” the beam; this means that the electrons bend a little when the field is applied, and exit the magnet with a different angle than they entered with. Since the undulators have a similar effect, the strength of the magnets can be adjusted to exactly compensate for the undulators, and the final result is an undisturbed orbit. This kind of compensation has been implemented for the NanoMAX and BioMAX undulators, and can now be used for all future insertion devices in the ring. The other negative effects of the undulators have been investigated, and at the moment, it seems like new measurement methods are needed to get the full picture of these disturbances. When the stronger devices are installed, this might become a problem. At the moment, however, the NanoMAX and BioMAX are able to operate without disturbing the beam, and the light they produce will soon be available to users eager to explore the capabilities of this new world-class facility. Hopefully, this will lead to new exciting discoveries and scientific development.

---

# List of Acronyms

---

**ID:** Insertion Device  
**IVU:** In Vacuum Undulator  
**LHC:** Large Hadron Collider  
**CERN:** European Organization for Nuclear Research  
**RF:** Radio Frequency  
**COD:** Closed Orbit Distortion  
**MML:** Matlab Middle Layer  
**AT:** Accelerator Toolbox  
**LOCO:** Linear Optics from Orbit Response  
**BPM:** Beam Position Monitor  
**BLM:** Beam Loss Monitor  
**FWHM:** Full Width Half Maximum  
**EPU:** Elliptically Polarized Undulator



---

# Table of Contents

---

<b>1</b>	<b>Introduction</b>	<b>1</b>
1.1	Aims of Project . . . . .	2
<b>2</b>	<b>Background</b>	<b>3</b>
2.1	Synchrotrons . . . . .	3
2.2	Beam Dynamics . . . . .	5
2.3	Insertion Devices . . . . .	9
2.4	ID Perturbations . . . . .	11
2.5	MAX IV Laboratory . . . . .	12
<b>3</b>	<b>Methodology</b>	<b>17</b>
3.1	Procedure . . . . .	17
3.2	Simulations . . . . .	17
3.3	Feed Forward Correction . . . . .	18
3.4	Measurements . . . . .	19
<b>4</b>	<b>Results</b>	<b>23</b>
4.1	Orbit . . . . .	23
4.2	Optics . . . . .	29
4.3	Beam Displacement Measurements . . . . .	30
<b>5</b>	<b>Discussion and Conclusions</b>	<b>32</b>
5.1	Feed-forward Generation . . . . .	32
5.2	Tune and Beta-Beat . . . . .	33
5.3	Beam Displacement Measurements . . . . .	33
5.4	Summary . . . . .	34
<b>6</b>	<b>Future Work</b>	<b>35</b>
	<b>References</b>	<b>36</b>

---

# Introduction

---



**Figure 1.1:** The MAX IV facility. [1]

On the 13th of June 2016, the MAX IV synchrotron facility was inaugurated in Lund, Sweden; a third generation light-source and the product of more than 30 years of local synchrotron science and development. A synchrotron produces highly energetic light for a variety of users within a vast range of scientific fields, from material science to archeology. This light is emitted by highly relativistic electrons circulating within a large storage ring. When the electrons are accelerated perpendicularly to their direction of motion, i.e. when their trajectory is bent, light is emitted. In modern synchrotrons, long arrays of permanent magnets, so called undulators or wigglers, are inserted into the ring; these Insertion Devices (IDs) bend the trajectory of the electrons into what resembles a slalom path, and the resulting light is emitted in a narrow cone in the forward direction. From there it is guided through a beamline to an experimental station. The IDs are essential to the operation of the synchrotron, but they also affect the stored beam in various unwanted ways.

This thesis work concerns the effects of the two first IDs installed in the MAX IV 3 GeV storage ring. The perturbations caused by the two In-Vacuum Undulators (IVUs) have been measured and methods for neutralization have been developed.

This report starts with a background section, outlining the theory of beam dynamics and ID perturbations, followed by a methodology section where the software and measurement techniques that have been used are described. After this the results and interpretations are presented, and finally there is a short discussion about possible future work.

## 1.1 Aims of Project

The aims of this master's thesis project were:

- To neutralize the effects of the two IVU's for the NanoMAX and BioMAX beamlines on the electron beam in the MAX IV 3 GeV storage ring, with respect to orbit distortion, tune shift and other non-linear effects.
- To develop an automated algorithm for the feed-forward correction of closed-orbit distortions cause by the IVU's, which should be compatible with variable optics configurations and future insertion devices.
- To characterize the magnetic properties of the two IVU's based on their effect on the beam.

## 2.1 Synchrotrons

This section introduces the basic principles which are crucial to understanding the function of a synchrotron. For a more detailed and thorough explanation of these topics, the interested reader is directed towards any entry level accelerator physics textbook, for example *The Physics of Particle Accelerators* by Klaus Wille [2].

### 2.1.1 Synchrotron Radiation

The acceleration of a variety of charged particles, from heavy ions to light electrons, has been possible for about a century. The first accelerators were built in the early 20th century mainly for the purpose of nuclear and particle physics. The most famous accelerator in the world, the Large Hadron Collider (LHC) at the European Center for Nuclear Research (CERN), is indeed a such a machine, colliding protons accelerated to enormous energies. In 1947, emission of light was observed for the first time from an electron accelerator, a synchrotron, and from there this type of radiation took its name. [3]

Synchrotron light can be observed when a charged particle is accelerated. The intensity of the radiation depends strongly on the energy of the particle, and is only easily observed when the particle approaches a relativistic speed, i.e. approaches the speed of light. Due to the relatively small mass of the electron, it is comparatively easy to accelerate an electron to an energy where synchrotron radiation can be observed compared to the heavier proton. While synchrotron radiation is produced by a particle accelerated linearly, it is many magnitudes stronger when the particle is accelerated in a direction not parallel to the velocity, i.e. when the particle path bends. The emission is most effective when the acceleration is perpendicular to the direction of motion. [3] Because of the enormous speed of the emitting particles, relativistic effects must be taken into effect to properly describe the resulting radiation. Figure 2.1 shows how the donut-shaped radiation in the electron's frame of reference turns into a narrow, forward-directed cone in the laboratory frame.

Originally, synchrotron radiation was considered primarily to be a problem, a damping effect on the high energies of low-mass particles. Today, however, synchrotrons are built with the express purpose of producing as much radiation as possible, despite their huge size and investment cost; a facility like MAX IV is gigantic

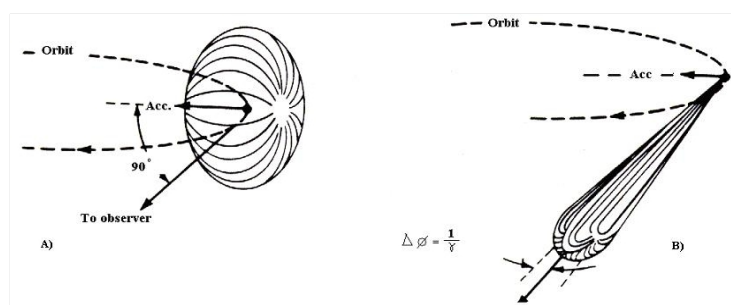


**Figure 2.1:** Visualization of the Lorentz transformation of emitted synchrotron radiation. Illustration by R. Bartolini. [4]

compared to a modern laser, which can be fitted onto a tabletop. They are still built because of the many desirable qualities of synchrotron light: high intensity, very broad spectral region, narrow angular collimation, a pulsed time structure, etc [3]. While most of these may also be achieved by a state-of-the-art-laser, the big advantage of a synchrotron is the broad spectral range of the resulting radiation. A synchrotron can produce radiation continually with a high repetition rate, brilliance and coherence, at energies currently unattainable by lasers. Especially the hard X-ray range (5-100 keV), is most easily achieved with a synchrotron. The energy is also tunable, allowing for spectroscopy experiments and the possibility to match the photon energy to a material or element transition energy. At peak operation, the MAX IV facility will continuously deliver light to approximately 30 beamlines, where different experiments may be performed simultaneously. [5] This versatility of the synchrotron motivates the large investment involved in building it.

### 2.1.2 Storage Rings

For the continuous production of synchrotron light, a continuous flow of high energy electrons is required. These electrons must then be accelerated perpendicular to their velocity.

In a synchrotron, electrons are first accelerated to relativistic speeds. This is commonly done using high gradient Radio Frequency (RF) fields. The process of acceleration results in a train of electron bunches, making up the electron beam. These electrons are guided to a storage ring, where they circle around in a vacuum tube. Magnets around the ring bend the path of the electrons and focuses the beam. In a modern synchrotron, the light is usually not extracted at these bending magnets, but in so called insertion devices. These are rows of permanent magnets that "wobble" the electrons back and forth. Due to the radiation emitted and other losses, the electrons lose energy as they orbit around the ring, and energy must be replaced in RF-cavities. This carefully designed equilibrium between energy loss, RF acceleration and magnet steering is the fundamental process of a storage ring. [2]

## 2.2 Beam Dynamics

In accelerator physics charged particles (electrons, protons, etc), are accelerated and guided by electromagnetic fields. The interaction between the beam and the accelerating and steering fields is referred to as particle *beam dynamics*. [6]

### 2.2.1 The Lorentz Force

The interaction between charged particles and electromagnetic fields is described by the Lorentz force:

$$\mathbf{F} = \frac{d}{dt}\mathbf{p} = q(\mathbf{E} + \mathbf{v} \times \mathbf{B}). \quad (2.1)$$

$\mathbf{E}$  and  $\mathbf{B}$  are the electric and magnetic fields,  $q$  is the particle charge and  $\mathbf{v}$  is the electron velocity. Knowledge of the Lorentz force allows for the prediction of the path of a charged particle through known magnetic and electric fields. This is the essence of beam dynamics, also called *beam optics*. In electron accelerators, the particles quickly become relativistic, i.e. velocity quickly approaches the speed of light:  $|\mathbf{v}| \approx |\mathbf{c}| \approx 3 \cdot 10^8$  m/s. This approximation can rarely be made when accelerating heavier particles or ions, due to their much higher mass. [2]

Integrating force with respect to the path length gives the change in kinetic energy:

$$\Delta E_{kin} = \int \mathbf{F} \cdot d\mathbf{s}. \quad (2.2)$$

Inserting equation 2.1 in 2.2, and knowing that  $d\mathbf{s} = \mathbf{v}dt$ , gives

$$\Delta E_{kin} = q \int \mathbf{E} \cdot d\mathbf{s} + \frac{q}{c} \int (\mathbf{v} \times \mathbf{B}) \cdot \mathbf{v} dt \quad (2.3)$$

The product  $(\mathbf{v} \times \mathbf{B}) \cdot \mathbf{v}$  disappears and it can be seen that the energy of the particle cannot be changed by the influence of magnetic fields. Magnetic fields change a particle's momentum but not its speed, i.e. only its direction. Thus magnetic fields can only be used for deflecting particles, while electric fields may also accelerate particles. [2] Theoretically, electric fields could also be used for steering purposes; usually, however, magnetic fields are used to guide particles in accelerators. This because the resulting force from the magnetic field scales with the velocity of the particle, i.e. for a relativistic particle, achieving the equivalent force from a magnetic field with the strength of 1T would require an electric field of  $\approx 300$  MV/m. Such field gradients are not achievable with today's technology, whereas a magnetic field of 1T is obtained with relative ease. [6]

### 2.2.2 Magnets

Most magnets in accelerators have very specific functions; dipole magnets for steering, quadrupole magnets for focusing, etc. Some magnets may combine two or more of these functions, but in modern synchrotrons they are most often separated. The pattern of magnets in an accelerator is called a *lattice*.

In the region close to the beam path there is high vacuum and any material effects can be neglected. The magnetic fields must then fulfill the Laplace equation:

$$\Delta V = 0 \quad (2.4)$$

where  $V(x, y, z)$  is the scalar magnetic potential. [6] The general solution can be expressed as a Taylor expansion, and when this solution is separated into multipole components, the fields corresponding to the most common magnets are found:

$$\begin{aligned} \text{Dipole} & \quad -\frac{e}{p} V_1 = -\rho_y x + \rho_x y, \\ \text{Quadrupole} & \quad -\frac{e}{p} V_2 = -\frac{1}{2} \underline{k} (x^2 - y^2) + kxy, \\ \text{Sextupole} & \quad -\frac{e}{p} V_3 = -\frac{1}{6} \underline{m} (x^3 - 3xy^2) + \frac{1}{6} m (3x^2y - y^3), \\ \text{Octupole} & \quad -\frac{e}{p} V_4 = -\frac{1}{24} \underline{r} (x^4 - 6x^3y^2 + y^4) + \frac{1}{24} r (x^3y - xy^3), \end{aligned}$$

where  $\rho_y$ ,  $\rho_x$ ,  $\underline{k}$ ,  $k$ ,  $\underline{m}$ ,  $m$ ,  $\underline{r}$  and  $r$  represent the strength of the multipole component. [6] Each multipole contains two terms, one oriented "normally" and one skew component; the term with an underlined constant is the skew field. For the dipole component, this simply represents bending in the  $x$  or  $y$  plane. Since the skew components introduce coupling between the two transverse planes, they are not used unless to specifically compensate for coupling introduced elsewhere. [6]

## Dipoles

Dipole fields bend the trajectory of the electrons. The pole shape of a conventional ferromagnet can be derived from the magnetic potential  $V = -\frac{\rho}{(e/p)}y$ , and corresponds to two horizontally parallel poles, where  $\rho$  is the bending radius of the magnet. This corresponds to a uniform field in the vertical direction,  $B_0 = \frac{(e/p)}{\rho}$ , causing horizontal deflection. [2]

Generally, the deflection angle in a magnetic field is:

$$\theta = \int \frac{1}{\rho} ds = \int \frac{B(s)e}{p} ds \quad (2.5)$$

If the field is uniform, as in a dipole, this simplifies to:

$$\theta = \frac{e}{p} B_0 L \quad (2.6)$$

Using a uniform magnetic fields, dipole fields, an electron beam can then be guided along a roughly circular periodic trajectory. Most storage rings consist of many bending sections separated by straight sections, and thus more closely resemble polygons than circles.

The easiest dipole model to mathematically describe is the sector magnet, where the electrons enter the magnet at the same longitudinal  $s$ -position regardless of transverse position. Due to the difference in distance traveled through the field for electrons with different horizontal entrance positions, this kind of magnet also causes a weak horizontal focusing. Many magnets are, however, instead of a rectangular type. In this case, the pole face causes so called *edge focusing*, resulting in a total vertical focusing and horizontal defocusing. [2]

## Quadrupoles

Quadrupole magnets are used to focus the beam. The magnetic potential  $V = -\frac{k}{(p/e)}kxy$  corresponds to a pole shape that can be seen in Figure 2.2. The field, and thus the effect on the beam, changes sign on different sides of the transverse axis, and thus acts as a focusing or defocusing force, see Figure 2.2. Note that a quadrupole field is always focusing in one plane and defocusing in the other. [2]

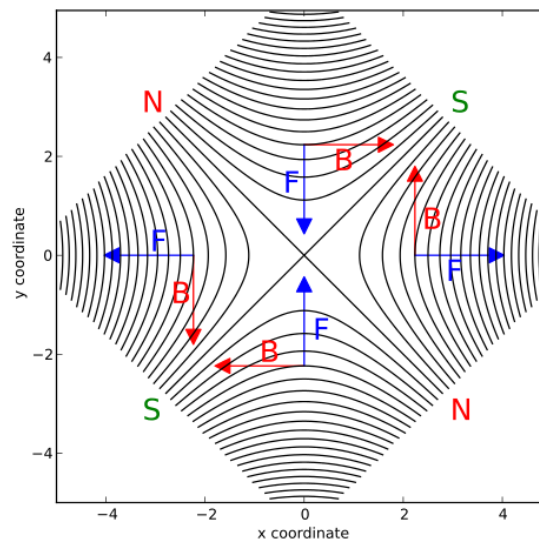


**Figure 2.2:** Magnetic field of a quadrupole magnet. [7]

## Sextupoles and higher Order Multipoles

In addition to steering and focusing magnets, modern synchrotrons also have to take into account dispersion effects arising from a non-uniform energy of the beam and other non-linear effects. Chromaticity, a measure of how sensitive the beam is to energy spread and energy deviations, can be adjusted via sextupole magnets, and octupole magnets are regularly used to reduce other non-linear instabilities. [2]

### 2.2.3 Equation of Motion

The equations of motions for a charged particle through a general magnet field can be derived from the Lorentz force in various ways. In the case of accelerator physics coordinates that are relative to the ideal path through the sequence of magnets in question are preferable, since this ideal path is stationary. The equations of motion are thus defined in a co-moving coordinate system  $(x, y, s)$ , where  $s$  is the longitudinal periodic coordinate along the ideal path, and  $x$  and  $y$  are the displacements in



the transverse plane. In such a system, a particle with a starting position  $x = y = 0$  would remain at that transverse position through the system indefinitely. This is not strictly true in the case of energy loss and gain, but serves as a good reference point. The position of a particle is often described in *phase space*;  $x$  denotes transverse displacement from the ideal orbit and  $x'$  the angular deviation. [2]

Generally, the equations of motion in the two transverse planes are the same, and can be expressed as:

$$u'' + k(s)u = 0 \quad (2.7)$$

where  $k(s)$  describes the evolution of the magnetic fields around the ring. This function is generally discontinuous and there is thus no general analytical solution. [6]

## 2.2.4 Betatron Oscillations

While the general equation of motion, 2.7, has no simple analytical solution, it closely resembles the harmonic oscillator. The following ansatz is made:

$$u(s) = \sqrt{\epsilon} \sqrt{\beta(s)} \cos(\phi(s) - \phi_0) \quad (2.8)$$

This is an oscillatory solution with initial phase  $\phi_0$ , and position dependent phase and amplitude  $\phi(s)$  and  $\sqrt{\epsilon\beta(s)}$ . The amplitude in turn consists of a constant factor  $\epsilon$ , usually called the emittance, and the so called  $\beta$ -function. Together, they represent the envelope or edge of the beam. The cos-term implies that the electrons oscillate within this envelope depending on their initial phase and position; these are called *betatron oscillations*. Generally,  $\beta(s)$  cannot be found analytically but must be numerically calculated. The  $\beta$ -function is one of the most important parameters of a synchrotron. It is a reflection of the focusing forces in the lattice and plays a role in determining many important beam parameters.[2]

Another very important parameter derived from equation 2.8 is the *tune*. This is a scalar describing the number of betatron oscillations an electron makes in one turn around the ring. If the  $\beta$ -function is known, the tune can be found analytically through:

$$\nu_{x,y} = \frac{1}{2\pi} \oint \frac{1}{\beta_{x,y}(s)} ds \quad (2.9)$$

Far from all tune points,  $(\nu_x, \nu_y)$ , are stable. Different multipole fields from different magnets induce different resonances; the dipoles cause integer resonances, quadrupoles half integers, etc. It is crucial to have good tune working point far from any strong resonances. In the same vein, a tune shift from the designated working point runs the risk of hitting a resonance and killing the beam. [2]

## 2.2.5 Linear Optics

The linear components of beam dynamics are the effects of dipoles and quadrupoles. Ignoring other components in equation 2.7, and assuming the particle is at the design energy and there is no bending in the vertical plane, the linear equations of

motion are [2]:

$$\begin{aligned} x'' + \left( \frac{1}{\rho(s)^2} - k(s) \right) x &= 0 \\ z'' + k(s)z &= 0 \end{aligned} \quad (2.10)$$

In many places around the ring, the dipole bending radius and the quadrupole strength is zero. That means that the variables  $\rho$  and  $k$  are discontinuous and the equations do not have a straight-forward analytical solution. However, for the path through a single magnet or through a drift section, a solution can be found. Solving for position,  $x(s)$  and angle  $x'(s)$  gives expressions for how these variables evolve over the length of the component given any initial conditions  $x_0$  and  $x'_0$ . Due to the linearity of the system, they can be written in matrix notation, and these matrices are called *transfer matrices*. Some examples are:

$$\begin{pmatrix} 1 & s \\ 0 & 1 \end{pmatrix} \text{ Drift section} \\ \begin{pmatrix} \cos \sqrt{|k|}s & \frac{1}{\sqrt{|k|}} \sin \sqrt{|k|}s \\ -\sqrt{|k|} \sin \sqrt{|k|}s & \cos \sqrt{|k|}s \end{pmatrix} \text{ Focusing quadrupole (k<0)} \end{pmatrix} \quad (2.11)$$

By multiplying the transfer matrices of the elements of a magnet array, the particle position at any place can be found if the initial position is known. Similarly, if the  $\beta$ -function is known at one point in the ring, the matrix method may be used to find it at all other positions. [2]

The matrix method may also be utilized for relations between other linear parameters of the beam; for example, a dipole error or kick has a linear impact on the orbit, and a quadrupole error or strength change has a linear relation to the tune. These relations can be summed into a *response matrix*:

$$\Delta \mathbf{x} = \mathbf{R}\boldsymbol{\theta}, \quad (2.12)$$

where in this case  $\boldsymbol{\theta}$  is the kick and  $\Delta \mathbf{x}$  is the orbit response. The transfer matrix  $\mathbf{R}$  is not necessarily quadratic. [6]

## 2.2.6 Dynamic Aperture

In a storage ring, particles in the beam naturally cannot survive if their oscillation amplitude exceed the size of the vacuum chamber, the physical aperture. The combined effects of non-linear fields and other dynamic effects also impose restrictions on the beams, resulting in "soft-walls" in the accelerator. This is the dynamic aperture, and it is defined as the maximum phase space amplitude within which particles do not get lost as a result of single-particle dynamic effects. [8] Non-linear fields from for example sextupoles may have severe effects on the dynamic aperture unless the lattice design takes this into account. [2]

## 2.3 Insertion Devices

The first synchrotrons used the light emitted from bending magnets in machines built for other purposes. While this light is still occasionally used, once synchrotrons

were built with the explicit purpose of producing synchrotron light, attempts to optimize the intensity and energy of the radiation resulted in more complex devices. These are inserted into the straight sections between the bending magnets and are therefore named insertion devices. [9]

### 2.3.1 Basic Principles

The idea of a modern ID is simple; instead of using a single bending dipole, many such dipoles are placed one after another, causing the electron to wiggle or undulate; hence they are also commonly known as undulators or wigglers. These arrays of dipoles are usually made of permanent magnets and are several meters long. Today, many kinds of IDs exist, able to produce light with different wavelengths, intensity and polarization. [9]

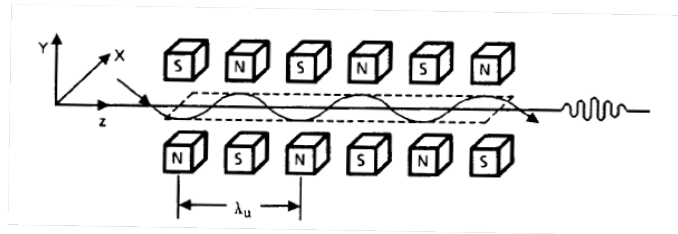


**Figure 2.3:** ID schematic view. Illustration by J. D. Jackson. [10]

There is no fundamental difference between the two categories of IDs. The underlying design is the same, but an undulator generally has a weaker field and thus displaces the electrons less than the stronger wiggler. Synchrotron radiation is emitted in a narrow cone with an angle of approximately  $\pm 1/\gamma$  and the direction of the cone is in the direction of motion of the electron. If the angular deviation of the electron's direction is less than the angular spread of the radiation cone, the radiation will overlap and the resulting spectrum consists of sharp spikes at a fundamental wavelength and harmonics. This is true for the weaker field of an undulator. For a wiggler, the spectrum contains more harmonics, until the eventually they blend together to one almost continuous curve. [11]

Light with different polarization may be produced by shifting the relative longitudinal position of the upper and lower magnetic array. This results in a corkscrew motion of the beam and the outgoing light becomes elliptically polarized to a degree relative to the longitudinal shift. These devices are referred to as Elliptically Polarized Undulators (EPUs). [9]

### 2.3.2 Insertion Device Radiation

In an undulator, the magnetic field can generally be assumed to be sinusoidal. On axis:

$$\mathbf{B} = B_0 \sin(k_u z) \mathbf{e}_y \quad (2.13)$$

where  $z$  is the longitudinal coordinate along the undulator axis. [11] From there, the motion of the electrons through the undulator may be derived, and in the moving

coordinate system the electrons will emit radiation like an oscillating dipole. By a Lorentz transformation to the laboratory frame, the so called undulator formula is found:

$$\lambda_n = \frac{\lambda_u}{2\gamma^2 n} \left( 1 + \frac{K^2}{2} + \gamma\theta \right), \quad (2.14)$$

where  $\lambda_u$  is the undulator period,  $\gamma$  is the relativistic gamma factor,  $n$  is the harmonic and  $\theta$  is the angle relative to the axis. [11] The  $K$ -factor is called the *undulator parameter* and is defined as:

$$K = \frac{eB_0\lambda_u}{2\pi mc}. \quad (2.15)$$

The only factor here which can be manipulated to change the wavelength of the light in 2.14 is the peak magnetic strength,  $B_0$ . Since IDs are built with permanent magnets, this is done by changing the gap between the upper and lower magnetic array. These changes alters the wavelength of the different harmonics, and in such a way the undulator radiation may be tuned to the desired energy. [11]

## 2.4 ID Perturbations

An IDs primary function is to produce synchrotron light, but apart from the energy loss of the electrons in form of radiation, the array of magnets also has several unwanted effects on the beam dynamics of the ring. To ensure stable operation, an ID must be designed in a manner that minimizes these effects, and those that cannot be avoided must be compensated for.

### 2.4.1 Orbit Distortion

A perfect ID has a perfectly symmetrical sinusoidal field, resulting in a perfectly symmetrical sinusoidal path of the electrons. If, however, there are any errors in the magnets, the path will deviate, and the beam will exit the device off-axis. This deviation may be in the form of a displacement,  $\Delta x$ , or an angle,  $\theta$ , or both. The extent of these errors can be measured by the magnetic field integrals over the length of the device. The first integral, the instantaneous field integrated over the longitudinal axis of the array, corresponds to a dipole effect, i.e. it gives the angle the electron will have upon exit according to 2.6. The second magnetic integral, the integration of the instantaneous value of the first integral along the same axis, gives the displacement from the axis of the particle upon exit. [9] The first integral can generally be assumed to have a larger effect, and in a simple approximation the undulator acts upon the orbit the same way a dipole kicker would. The effect of a kick on the closed orbit at a point location is easily calculated to be [9]:

$$\Delta x = \frac{\Delta x'_{kick} \sqrt{\beta(s)} \cdot \beta_{kick}}{2 \cdot |\sin \pi\nu|} \cos(\pi\nu - |\phi(s) - \phi_{kick}|) \quad (2.16)$$

Theoretically, these field integrals can be reduced to zero, resulting in a completely transparent device. Practically, this is almost impossible. The field errors

also change for different gaps of the ID, and all gaps cannot thus be rendered transparent. While it is important to have well-constructed IDs that minimize these integrals, a well-functioning orbit correction scheme is needed.

## 2.4.2 Impact on Optics

Even if the magnetic integrals could be eliminated, a perfect ID still gives rise to a focusing effect [9]. This can be understood as a combined effect of the edge focusing of a large number of rectangular dipoles. The wiggle of the electron path causes the particles to enter into each dipole field with an angle, which causes an edge focusing. Over several periods, this adds up to a significant vertical focusing and the horizontal focusing usually cancels. [6] Numerically, the tune shift can be expressed as [12]:

$$\Delta\nu_y = \frac{\beta_y L}{8\pi\rho^2} \quad (2.17)$$

More generally, the focusing may be derived from the Hamiltonian of the system and perturbation theory [13, 6], but the approximation in equation 2.17 is enough for the scope of this project. The tune shift is also related to the so called beta-beat, small oscillations in the amplitude of the  $\beta$ -functions. Generally, the beta-beat is given by [9]:

$$\frac{\Delta\beta}{\beta} = \frac{2\pi\Delta\nu}{\sin(2\pi\nu)} \quad (2.18)$$

## 2.4.3 Higher Order Perturbations

In a real ID magnetic array, the field is not perfectly sinusoidal at all places. The pole faces are not infinite, and off axis there can be noticeable edge fields. Any construction flaw or misalignment can result in complex higher order fields or skew components which may have a noticeable effect on the beam. These higher order components can have an impact on the dynamic aperture and lifetime of the beam. [12] The skew components couples the vertical and horizontal planes and causes a blow up of the vertical beam size. All these components are expected to be minimal at the exact center of the device, where the symmetry cancels many of them.

## 2.5 MAX IV Laboratory

The MAX IV Laboratory is a third-generation synchrotron light source in Lund, Sweden. The project was approved in 2010 and the facility was inaugurated in June 2016. [5] It will, once completely finished, consist of a linear accelerator delivering high energy electrons to two storage rings, one with an electron energy of 1.5 GeV and one with 3 GeV, as well as a short pulse facility. Figure 2.4 shows the layout of the facility. This section will cover the basic design of the 3 GeV ring and the NanoMAX and BioMAX beamlines relevant to the project.

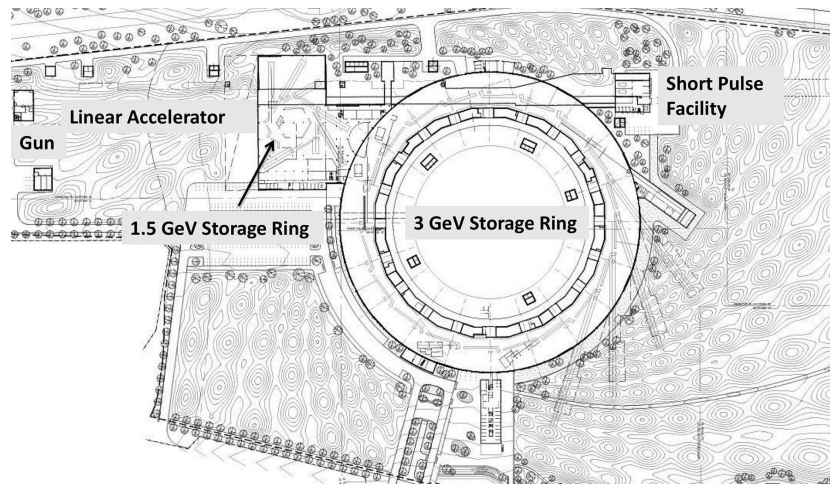


Figure 2.4: Layout of the MAX IV facility. [14]

### 2.5.1 3 GeV Storage Ring

The 3 GeV storage ring has a circumference of 528 m, divided into 20 *achromats*, identical sections of arrays of magnets which make up the lattice of the machine. The achromats are connected by 5 m long straight sections. One of the main features of the MAX IV big storage ring is its ultralow emittance, 0.33 nm horizontally, made possible by using the concept of multibend achromats. The number of strong magnets required for this design implies that the magnets must be extremely compact. This means the large ring has a smaller than usual vacuum chamber and very small magnet apertures. Many of the magnets are also built using a common iron block, reducing alignment errors. [15]

Figure 2.5 shows a schematic view of the lattice of one achromat. Four different kind of magnets are marked. Apart from these, each section also has 10 horizontal and 9 vertical corrector magnets, and 10 BPMs in each plane, as well as numerous other diagnostic equipment. The undulators are inserted in between each of these achromats. Figure 2.6 shows the  $\beta$ -functions of the bare lattice. The pattern should, ideally, repeat itself over each achromat, making the complete  $\beta$ -functions completely symmetrical. The design tune is 42.20 horizontally and 14.28 vertically [16].

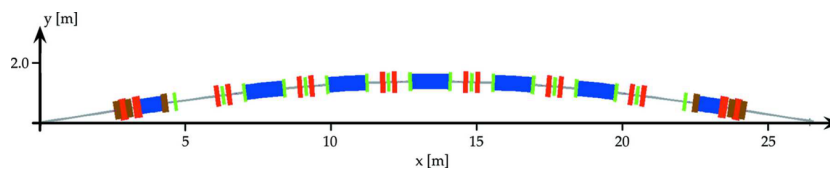
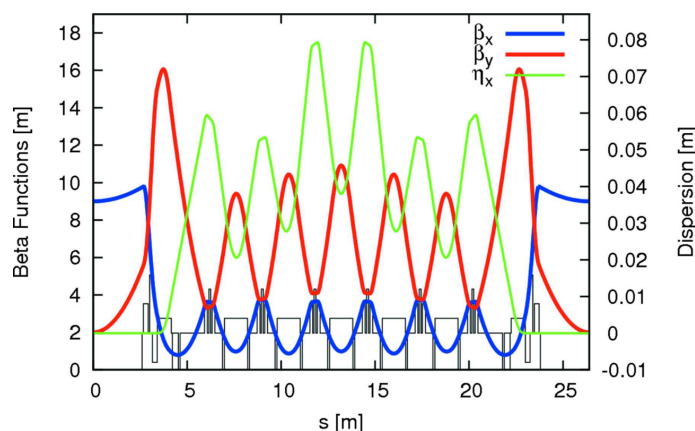


Figure 2.5: Schematic view of one achromat. Magnets indicated are gradient dipoles (blue), focusing quadrupoles (red), sextupoles (green) and octupoles (brown). [14]



**Figure 2.6:** Horizontal and vertical beta function over one achromat. In the figure the dispersion function can also be seen, which has no direct relevance for this project. [14]

## 2.5.2 Beamlines

In 19 of the straight sections there is room for an ID delivering light to a beamline and one or more experimental stations. Seven of the beamlines are scheduled for installation during the first phase of construction, and the two first are NanoMAX and BioMAX. BioMAX is placed in section 12, in the straight section between achromat 11 and 12, and NanoMAX in section 3, between achromat 2 and 3.

### BioMAX and NanoMAX

The BioMAX beamline is built for hard X-ray crystallography of bio-molecules and the NanoMAX beamline for hard X-ray imaging with a spatial resolution down to 10 nm [17, 18]. The requirements on the source are very similar, and therefore the undulators for the two beamlines have been identically designed. They are both in-vacuum undulators, meaning the magnet array is placed inside the vacuum chamber instead of outside. This allows for the undulators to be closed to much smaller gaps. The characteristics of the two IVUs are listed in Table 2.1.

Period Length	18 mm
Overall length of magnetic array	2 m
Gap range	38-4.2 mm
Maximum K-value	1.95
Energy range	5-30 keV

**Table 2.1:** Design parameters of the IVUs.

Both undulators were tested for compliance with specifications before installation in the ring. Most relevant for this project, the first and second magnetic field

integrals were measured using an in-vacuum Hall probe and moving wire measurements, to ensure they fell within error margins. Figures 2.7 and 2.8 show the first integral measurements done at MAX IV for both undulators for the full range of gaps. The plots show the integrated field in Gauss cm (1 Gauss or G. equals  $10^{-4}$  T) at different lines parallel to the longitudinal axis, where each colored line is a different gap. The results fall roughly within the allowed range of  $\pm 100$  G.cm, marked with dashed black lines, for all gaps but the very smallest, and there is no severe difference between the two undulators. These values are achieved after trimming the magnetic array to get as close to a zero magnetic integral as possible. Measurements were also done at the location of manufacturing, and it's worth noting that after transport, the measurements look different, demonstrating how sensitive the magnetic array is.

Another aspect to consider when looking at these plots is the earth magnetic field. In Lund the earth's field is approximately 0.5 Gauss [19], which over the 2 m long undulators corresponds to a magnetic integral of approximately 100 G.cm. The earth magnetic field is then if the same order of magnitude as the field errors. The undulators are also oriented differently in the ring, meaning the earth field affects them differently. This environmental difference of the two devices is thus likely to be as notable as the intrinsic variations.

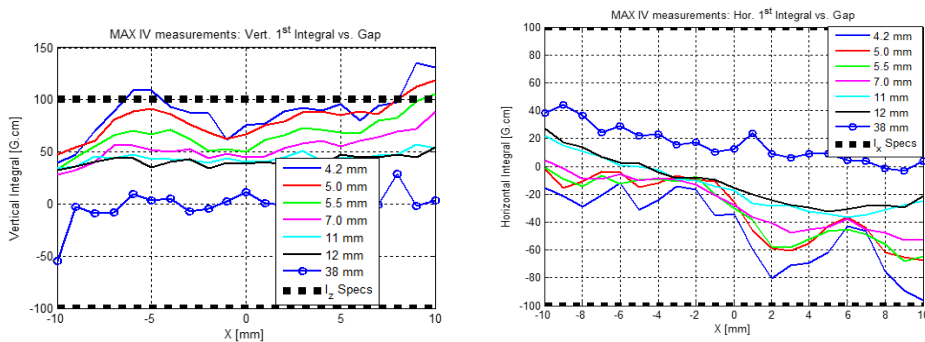


**Figure 2.7:** First magnetic integrals for different gaps and horizontal position, BioMAX. [20]

The two devices are equipped with four corrector coils, one pair at the entrance and one at the exit. These coil pairs are specifically designed to have a negligible hysteresis effect, which means that the relation between field strength and current is absolute. This is not true for the other electromagnets in the machine with an iron yoke. The coils are able to produce, independently in the two transverse planes, a kick corresponding to an integrated field of 400 G.cm over 5 A, with a linear excitation curve. This allows for any current through the correctors to be translated to an integrated field and compared with the field integral measurements. [20]



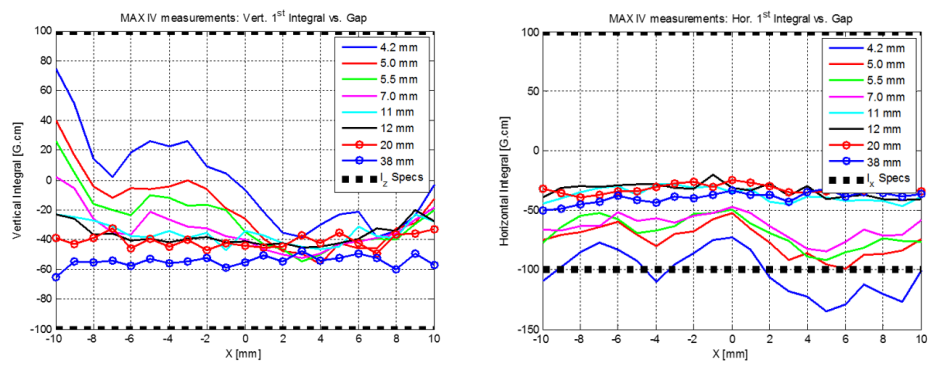


**Figure 2.8:** First magnetic integrals for different gaps and horizontal position, NanoMAX. [20]

## 3.1 Procedure

To achieve the goals listed in section 1.1, the following procedure was followed.

- A simple undulator model and some initial simulation tests were made in order to acquire working knowledge of the machine and gain experience with the software.
- The undulators were closed as far as possible without any compensation, neither feed-forward nor feedback. Effects on tune and orbit were measured.
- These measurements were replicated in simulations, and an algorithm for correcting the orbit was developed and tested on the simulation model.
- The algorithm for feed-forward generation was tested on the machine, and after being debugged, feed-forward tables were acquired for all gaps possible.
- With the orbit feed-forward and feedback on, beam displacement measurements were carried out to measure effects on beam size and lifetime.

The following sections will describe in more detail the different components of this procedure.

## 3.2 Simulations

### 3.2.1 Tools

#### The Matlab Middle Layer

The 3 GeV Ring at MAX IV uses a TANGO integration layer, which is corrected to a Matlab Middle Layer (MML) [16]. All simulations and measurements in this project have been made with this system. Matlab has been used for accelerator control and simulation at the ALS since the 1990's, and is today used at several machines around the world [21]. It is suited to this purpose due to reliability, matrix orientated computing, and platform independence [21, 22]. The MML is structured in such a way that the same scripts may be run on both the online machine and the simulator tracking codes, in this case the Accelerator Toolbox [21].

## Accelerator Toolbox

Accelerator Toolbox (AT) is, unlike most other accelerator codes, not a stand-alone program but a Matlab plugin, or toolbox. AT can be used to simulate particle motion through sequences of elements, and calculate beam and accelerator parameters, taking advantage of Matlab's extensive maths library and graphics tools. [23]

## LOCO

LOCO (Linear Optics from Orbit Response) is a code developed for NSLS X-Ray Ring to precisely determine the linear optics, including normal and skew quadrupole components, calibration of steering magnets, and more [24]. Knowing the magnetic configuration of a storage ring lattice, the response matrix can easily be determined; LOCO reverses the process. By measuring the response matrix on the actual machine and then iteratively modifying a simulated model using  $\chi^2$ -minimization, the magnet properties may be found. A thorough understanding of these properties is required to maximize the performance of the accelerator and also to be able to accurately predict measurements [24]. While originally written in FORTRAN, the code has been adapted to Matlab and AT [25]. It is regularly used at the MAX IV Facility.

### 3.2.2 Simulation Choices

For simulating the orbit distortion and orbit correction, the insertion devices were simulated within AT as two kicks, one at each end of the insertion device, in both the horizontal and vertical plane. The two kicks can reproduce any translation and angle of the beam given by the device, and thus reproduce the effects of any integral field errors.

## 3.3 Feed Forward Correction

The strategy for neutralizing the effects of the IDs on the orbit at the MAX IV 3 GeV ring was as follows. For the orbit, a set of air coils were used to correct for any field integral variations and resulting Closed Orbit Distortion (COD). A feed-forward scheme was set up for these coils, and after the feed-forward table is applied, the IDs will apply no kicks or translations to the beam [26]. The optics perturbations arising from the vertical focusing, the tune shift and beta-beat, were to be neutralized in two steps; a local correction where the gradients of the flanking quadrupoles were to be adjusted via a feed-forward table and a global adjustment via feedback, ensuring a stable working point for all gaps. [27]

### 3.3.1 Automated Feed-Forward Table Generation

The feed-forward tables required for orbit correction would be cumbersome to measure manually. Having an automatized method for acquiring these tables is essential to a smoother commissioning process for future IDs, and thus a goal of this project was to create such a method. The algorithm was structured as follows:

1. Measure the orbit, i.e. readings from the Beam Position Monitors (BPMs).
2. Apply a field in one plane in one of the correctors, i.e. kick the beam.
3. Measure the orbit response for a kick by each corrector in each plane.
4. Since the orbit distortion depends linearly on the applied kicks, find the matrix relating magnet strength to BPM positions, i.e. the response matrix from section 2.2.5
5. Change the ID setting, in this case the gap, causing an orbit distortion.
6. Measure the orbit distortion.
7. Solve the system of equations to find the required kicks in the correctors to counteract the orbit distortion from the ID.
8. Repeat from 2 for all gaps.

### 3.3.2 EPU Feed-Forward Generation

The future IDs to be installed in the ring involves several EPUs, which also have a variable phase offset in order to change polarization of the radiation. These devices then require a two dimensional feed-forward table; one value for every combination of gap and phase. Particularly the HIPPIE EPU was taken into consideration, since due to its length the corrector coils are integrated into the structures upholding the magnetic array. This means that the coils move, and the effective field strength varies with gap. The coils are also connected to the power supplies so that powering up one supply does not result in a pure field in either plane, but rather a skew field. To achieve a pure horizontal or vertical field all four coils must then be powered together with a ratio that differs with gap. The geometric factors which determines this ratio have been measured and the feed-forward generation algorithm was adapted in order to also be usable with this special configuration.

## 3.4 Measurements

### 3.4.1 Orbit

The orbit of the beam is measured with BPMs, of which there are 200 in the 3 GeV ring; 20 in each achromat. The BPMs are able to determine the position of the beam to within approximately  $0.3 \mu\text{m}$  rms certainty, even though the accuracy decreases with current. [16] All measurements were done relative to a pre-defined orbit. At the start of the measurements, the orbit was corrected using the slow orbit feedback towards the desired orbit for the optics configuration. The feedback was then turned off, and the instantaneous BPM values were recorded.

### 3.4.2 Tune

Two methods were available for measuring the fractional tune of the machine, one automated method using the MML, and one using a spectrum analyzer. Both involve exiting the beam, causing problems when running at possibly unstable configurations [16]. The spectrum analyzer, although a measurement done manually and thus much slower, disturbs the beam less and was thus used in most cases.

### 3.4.3 Orbit Bumps and Beam Displacement Measurements

To attempt to probe the higher order perturbations of the undulators, measurements need to be made for beam positions off-axis in the device. By defining an orbit with an offset over the undulator, and then letting the slow orbit feedback correct towards that orbit, a local bump in the orbit may be created. By changing the offset of the bump, the beam can be scanned over the horizontal axis of the ID.

To measure ID perturbations other than orbit distortion, two measurements were available; a beam loss monitor and a diagnostic beamline showing the synchrotron light from one of the bending magnets. When this work was carried out, all diagnostic equipment for these measurements were not yet installed and/or calibrated. Data thus had to be retrieved as screenshots and then analyzed manually.

#### Beam Loss Monitor

The Beam Loss Monitor (BLM) is situated after the BioMAX IVU and consists of two diodes, placed on opposite sides of the vacuum chamber. These diodes measure incident electrons on the vacuum pipe, i.e. scattered electrons just after the undulator. If there are any strong multipole fields in the ID, or any other perturbation that increases beam loss, most of these electrons can be expected to be lost right after the ID, some of them hitting the diodes. The measurement does not directly relate to the lifetime since it measures only lost electrons in one location. While doing the beam displacement measurements, the current in the ring needs to be low to protect the machine in case of beam loss. This is referred to as using a cold beam. At those currents, of  $<3.5$  mA, the lifetime measurements have huge fluctuations, and are thus not reliable. The BLM is then the only indication of lifetime available.

Figure 3.1 shows an example of a BLM reading. Both injection and controlled reduction of current can be seen. Injection was started at approximately 8:45 and can be seen clearly as a large increase in registered electrons. At about 8:51 the current of the machine was reduced slowly to achieve cold beam status, which can be seen as a smaller spike in measured electrons. Many more electrons are lost during injection than during current reduction because of low injection efficiency, i.e. a large portion of the injected electrons never find a stable orbit.

#### Beam Size Measurement

The change in beam size was estimated using the diagnostic beamline, where the visible synchrotron light from one of the bending magnets can be used to determine beam size and emittance [28, 29]. The image on the screen depends on the size of

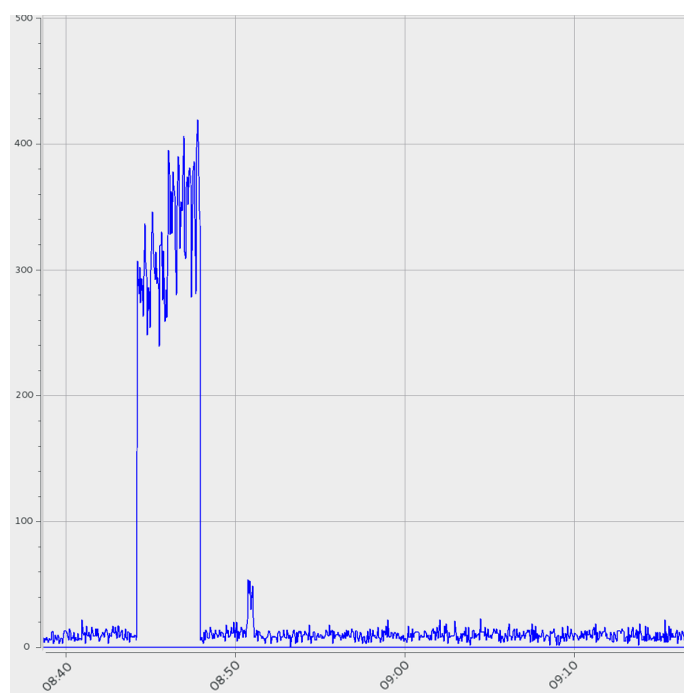


**Figure 3.1:** BLM sample results. The plot shows time vs. counts, i.e. scattered electrons hitting the diodes.

the electron beam, and any change in beam size should be proportional to a change in the image. Proper analysis of the image data was not implemented at the time the measurements were done, and thus the data was acquired in the form of images such as the one seen in Figure 3.2. The image on the CCD screen can be seen at the left. Several side lobes are noticeable, especially in the vertical direction, due to refractive effects of mirrors and apertures. To the right a vertical and horizontal cross-section can be seen. These were analyzed to extract information of the FWHM. For this project, information about relative change was desired, not absolute size, and therefore no attempt at extracting a number for the beam size was made.

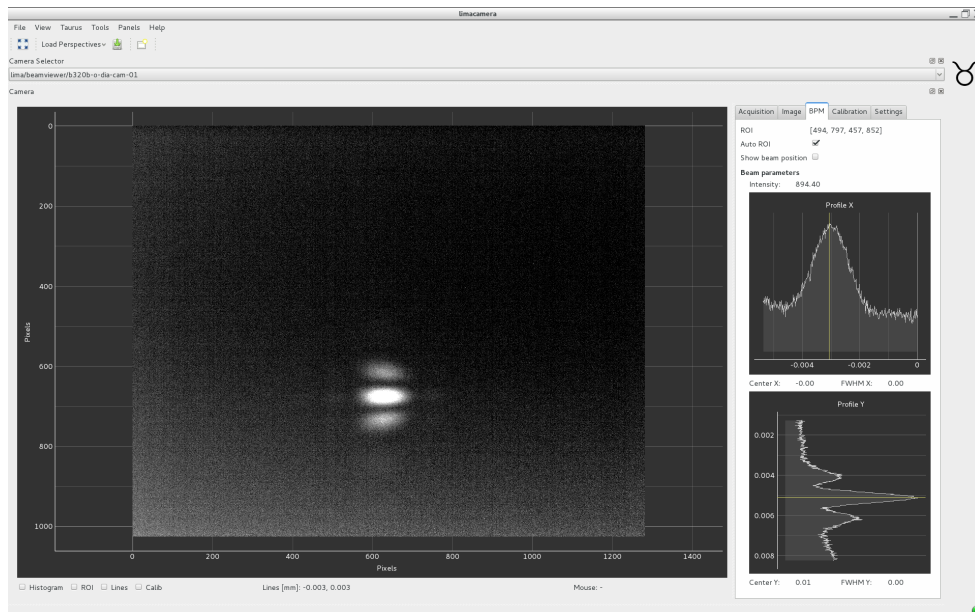


**Figure 3.2:** A screenshot of the information available from the diagnostic beamline.

## 4.1 Orbit

This section presents all results regarding the orbit measurements and orbit corrections, including the feed-forward table generation.

### 4.1.1 Initial Simulations

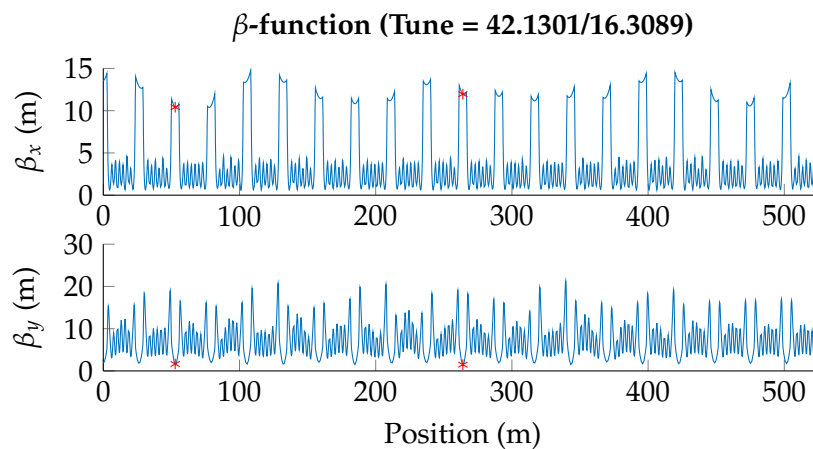


**Figure 4.1:**  $\beta$ -functions extracted from the LOCO fit. The stars mark the ID locations; NanoMAX first and BioMAX second.

For accurate simulations, the AT model was fitted using LOCO. Figure 4.1 shows the resulting  $\beta$ -functions around the ring. The location of the NanoMAX and BioMAX beamlines are marked with stars. There is a clear asymmetry in the  $\beta$ -functions at the optics configuration used. By altering the strength of the focusing elements this configuration can be changed, and the goal is a configuration that results in completely symmetrical  $\beta$ -functions. At the location of the BioMAX, the horizontal  $\beta$ -function has a value of about 12 m, compared to the design value of approximately



9 m, which can be seen in Figure 2.6. The  $\beta$ -functions over the two undulators are different, and they are not symmetrical locally over either device.

The undulators were modeled as two kicks, one in each plane, at the entrance and exit of the device, and two correctors were inserted in the AT lattice at the corresponding positions. The previously measured residual integrals, see sections 2.5.2, were translated to kicks and the resulting COD was calculated. In the initial phase an analytical approach was used. The tunes,  $\beta$ -functions and corresponding phase was extracted from the LOCO model in Figure 4.1, and the resulting orbit was found through equation 2.16. The kick was here assumed to be equally distributed across the undulator, i.e. half of the kick was applied at each end of the undulator.

Figures 4.2 and 4.3 show the simulated closed orbit distortion for both undulators and both planes. Notable is the y-plane distortions from the NanoMAX, where the kick changes sign compared to the open position - this results in the orbit being displaced in first one direction and then swing over in the other direction.

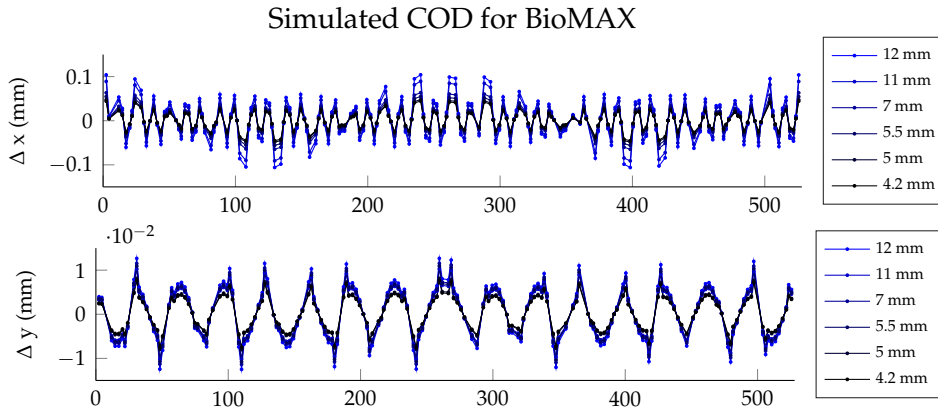


**Figure 4.2:** Simulated COD for BioMAX.

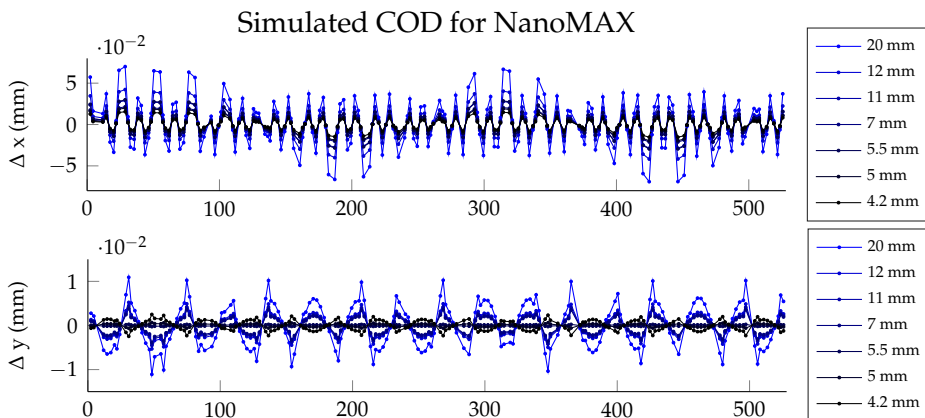


**Figure 4.3:** Simulated COD for NanoMAX.

### 4.1.2 Initial Measurements

Initial measurements were done on both the NanoMAX and BioMAX IVU at the end of April. The undulators were closed iteratively and at each gap the BPM positions were saved. The BioMAX undulator was closed to a 7 mm gap, after which the beam was lost during a tune measurement. The resulting COD can be seen in Figure 4.4. A clear linear growth can be seen in the vertical plane, once the distortions grow larger than the BPM noise level at about a 16 mm gap. In the horizontal plane the COD grows until approximately the 10 mm gap, when it starts to diminish again.

The NanoMAX undulator was closed to a 10 mm gap. Smaller gaps were avoided due to the risk of damaging the magnetic array during beam loss similar to the one experienced with BioMAX. The resulting COD can be seen in Figure 4.5. The linear growth of the orbit distortions can be seen in the horizontal plane, while in the vertical plane, the displacement barely reaches above the noise level even at the smaller gaps and the pattern is less pronounced. Note that the scale of the y-axis in the vertical plane for NanoMAX is one order of magnitude smaller than the others.

When comparing the two, it is clear that the BioMAX causes a bigger orbit distortion than NanoMAX. Overall, the measurements show a smaller effect than the simulations based on integrated field measurements. Comparing the orbit pattern of simulations and measurements, however, they show a clear similarity, and it was clear that the simple kick model was able to closely reproduce the COD from the real undulators.

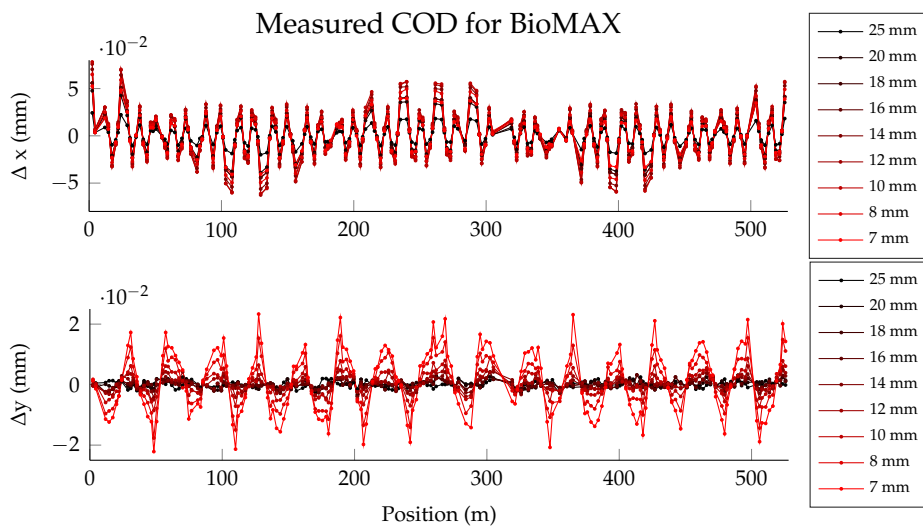


**Figure 4.4:** Measured COD for BioMAX.

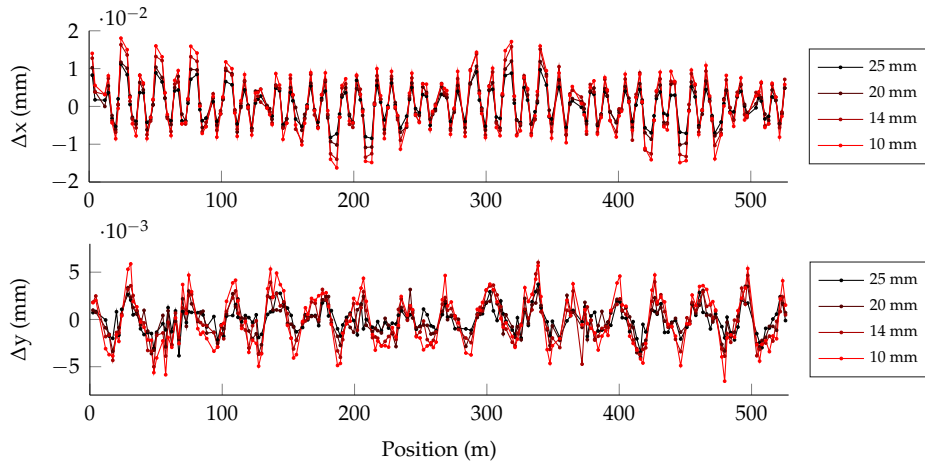


**Figure 4.5:** Measured COD for NanoMAX.

### 4.1.3 Feed-Forward Simulations

The algorithm for feed-forward table generation was written and tested in simulations according to 3.3.1. Figures 4.6 and 4.7 show the comparison between the measured COD and the corresponding found through the algorithm. For the larger gaps the correspondence is poor, especially in the vertical direction, but the match is very good for the lower gaps. The initial bad matching is due to the fact that the COD is on the level of the BPM noise, and thus the COD pattern measured is neither reliable nor reproducible.

### 4.1.4 Feed-Forward Generation

After successfully running the algorithm in simulations, it was tested on the real machine. Figures 4.8 and 4.9 show the final feed-forward tables as well as a plot of the corrector currents vs. gap. These values of current through the correctors were able to reduce the COD to the level of the BPM noise for all gaps. In the plot the values from the previous simulations are also shown, i.e. the calculated currents to neutralize the COD from the initial measurements. The trend from the simulations remains, even though the values do not exactly match. Since the LOCO fit of the machine does not exactly reproduce all effects in the machine, this is to be expected.

### 4.1.5 Magnetic Integrals

Figure 4.10 shows the two corrector kicks for each device and plane added and recalculated to the corresponding integrated field. The integrated field measurements have been rescaled to zero at max gap, to be comparable to the feed-forward generation results. This because all feed-forward generation tests were made in relation to a corrected orbit at max gap. The data from the integrated field measurements in the center of the devices are also plotted for comparison. It can be seen that to compen-

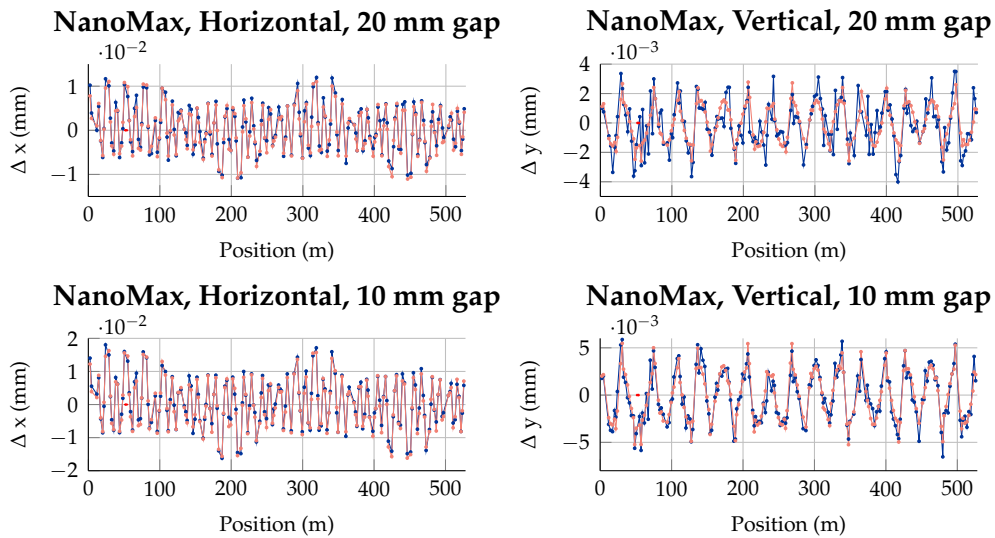


**Figure 4.6:** Matching of simulations to measurements. Dark blue: measured COD, and light red: simulated COD.

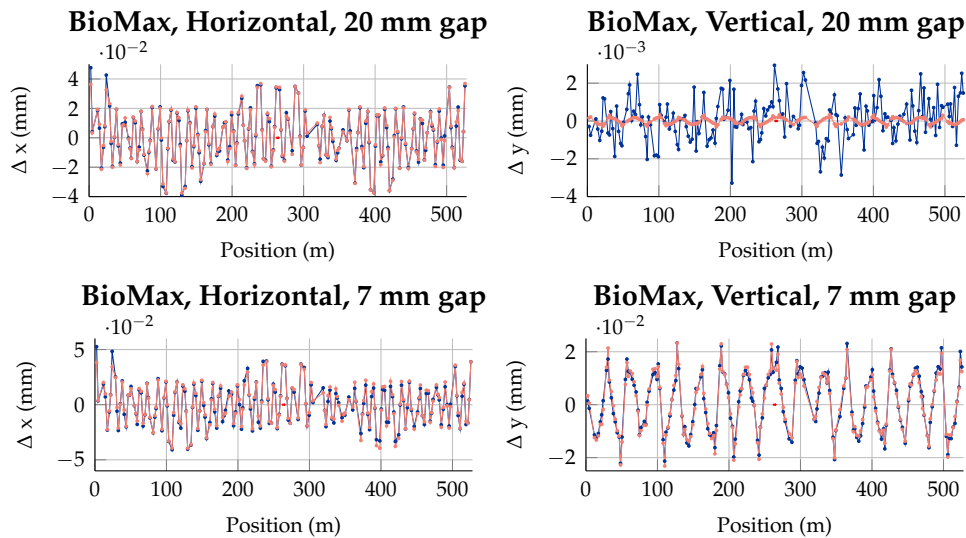


**Figure 4.7:** Matching of simulations to measurements. Dark blue: measured COD, and light red: simulated COD.

sate for the COD, a total kick on the same order as the integrated field is required, as expected. The notable deviance is the horizontal field integral for the BioMAX undulator, which seems to have the opposite sign of the previous measurements. The BioMAX correctors which supply a vertical field, i.e. corrects the horizontal orbit,

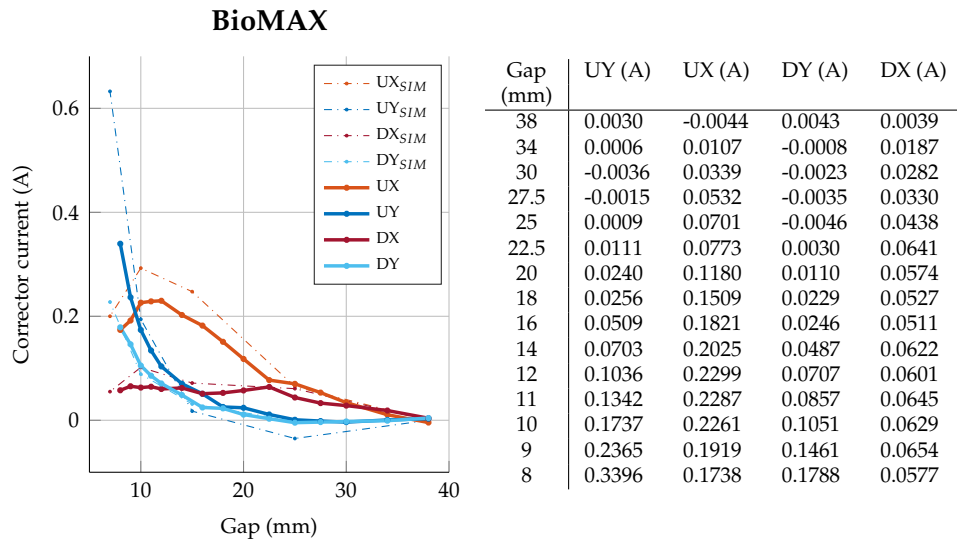


**Figure 4.8:** Simulated and final corrector current values. The table to the left shows the final feed-forward table.

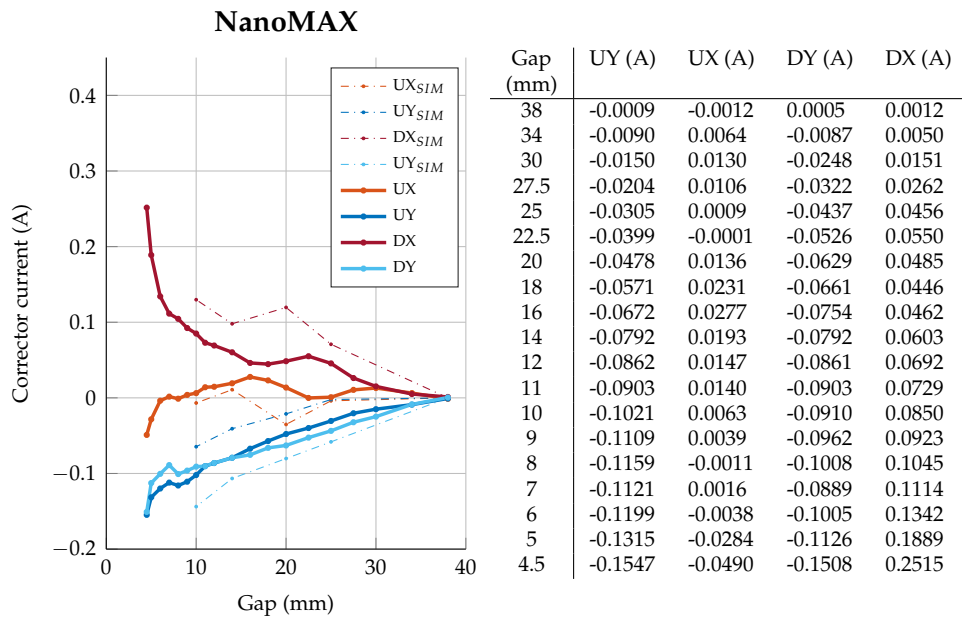


**Figure 4.9:** Simulated and final corrector current values. The table to the left shows the final feed-forward table.

also seem to require less current as the gap increases after the 10 mm gap. Since the measurements could not be completed, it is hard to tell if this is just a bump or if the

trend would continue. If it would, this is also in sharp distinction from the previous measurements, which show a significant increase in integrated field at the smallest gaps.

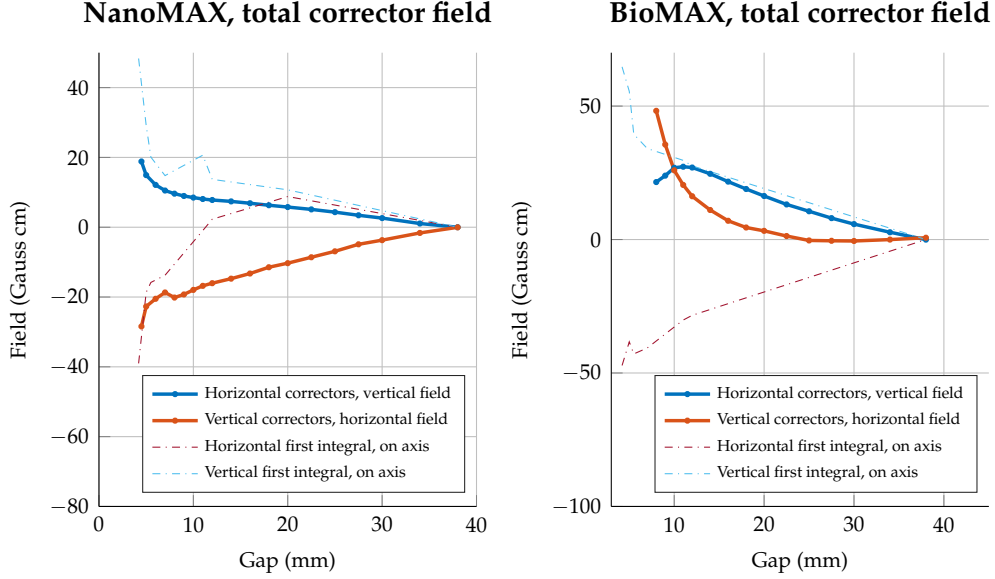


**Figure 4.10:** Total integrated field from corrector magnets compared to wire scan measurements.

## 4.2 Optics

The tune was measured during the initial orbit measurements, during the final feed-forward generation tests, and while closing the undulator with the feed-forward and feedback online.

### 4.2.1 Calculations

Based on the LOCO model and the physical data of the undulator, the tune shift was estimated to be, using the definition of the bending radius and the undulator parameter and according to equation 2.17:

$$\Delta\nu_y = \frac{\beta_y L}{8\pi\rho^2} = \left(\frac{e}{p}\right)^2 \frac{\beta_y L B^2}{8\pi} \approx \frac{\beta_y K^2 \pi}{2\gamma^2 \lambda_u^2} \approx 3 \cdot 10^{-4} \beta_y K^2 < 10^{-3} \quad (4.1)$$

Since the maximum undulator parameter is  $K \approx 2$ , and the vertical  $\beta$ -function over the undulator is not larger than two, the tune shift should not be noticeable before the third digit. This is at the edge of what the measuring equipment can reliably detect, and therefore any noticeable tune shift for these weak devices would probably be caused by some higher order perturbation in the device.

## 4.2.2 Measurements

No notable tune shift could be detected during any measurement. Due to this and reproducibility problems with the tune, it was decided that the feed-forward would not be implemented. The lack of a reliable non-destructive tune measurement would also make the algorithm hard to test.

## 4.3 Beam Displacement Measurements

The beam displacement measurements could unfortunately not be carried out to the full extent of what was planned. The goal was to scan the device with the electron beam in a  $\pm 10$  mm range in the horizontal plane. However, only about a tenth of that range was achieved. To create a local bump of the orbit, in this case over the undulator, requires at least four strong kicks. The corrector magnets quickly saturated to maximum current levels when asked to produce these bumps. In the end only ranges of  $+1.2/-0.5$  mm over BioMAX and  $+0.6/0.7$  mm over NanoMAX were possible.

In the range available for measurements, no change could be noted on the beam size monitor. Figure 4.11 shows the analyzed images from measurements on BioMAX in both planes. Both the initial position and the maximum bump are shown. The FWHM is marked in green and the value given is in pixels since only relative values were of interest. No variations beyond the error range can be seen.

Attempts to measure the tune were initially made, but were abandoned due to beam loss when exiting the beam. No changes were seen on the measurements which were done.

The BLM showed no variation while moving the beam transversely. Figure 4.12 shows a slight bump at approximately 09:17, corresponding to when BioMAX was closed to an 8 mm gap. No increase was seen before this when closing the undulator and none could be seen afterwards while attempting to bump the beam. This increased scattering at 8 mm coincides with the problems of closing this undulator to smaller gap than this.

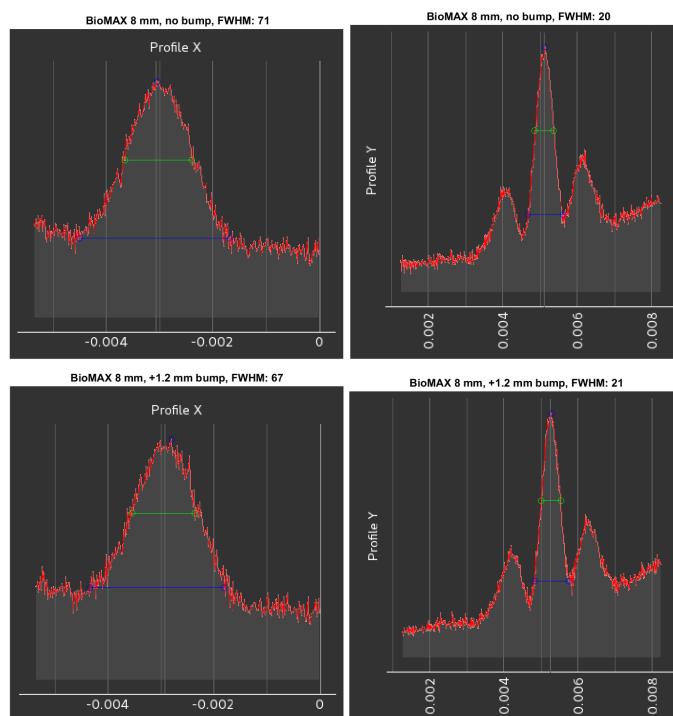


Figure 4.11: Beam size analysis.

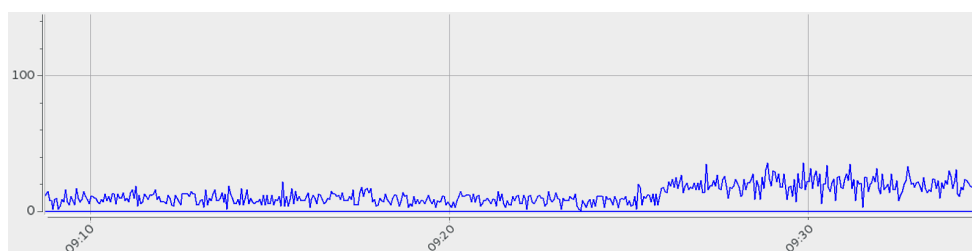


Figure 4.12: BLM during BioMAX measurements.



---

## Discussion and Conclusions

---

Overall the information about the IVUs that was gained from this project is in accordance with what was expected from previous measurements and estimations. There is however a difference between the two devices which was not expected from the data known prior to installing the devices in the ring. Consistently the BioMAX seems to have a more severe impact on beam dynamics than NanoMAX. At this time, it is difficult to say what the reason for this might be. One thing that must be taken into account is the non-ideal optics the ring was operating with during the time of this project, with a large degree of asymmetry in the  $\beta$ -functions both globally and locally over the devices. The undulator which has the worse behavior, BioMAX, has also experienced other troubles, such as difficulties with the gap and taper control. The cause of these problems could not be investigated during the time of this project since it would require machine shutdown, and thus how it affects the behavior of the device is hard to speculate about.

### 5.1 Feed-forward Generation

Except that the BioMAX IVU could only be closed to 8 mm due to the problems previously mentioned, acquiring the feed-forward tables for the two devices has been successful. The algorithm for feed-forward table generation has been implemented and runs in a time efficient manner with good results. After implementing the feed-forward compensation, the IVUs can be closed to the currently attainable smallest gaps without any noticeable COD. The currents required to achieve this compensation are well within the capacity of the correctors; for NanoMAX, which was closed to the absolute minimum gap, less than 5% of the maximum current was required. The BioMAX IVU requires more than that; at 8 mm gap, it already needs more current than the NanoMAX IVU at minimum gap. The steep increase in current needed as the gap is closed, especially by the vertical correctors, suggests that much stronger currents might be needed. Still, only 10% of the maximum current is used at 8 mm. The strongest corrector for NanoMAX only doubles its current value between 8 mm and 4.5 mm gap, and so there is no reason to believe the correctors for the BioMAX will saturate as the smallest gaps are obtained.

The BioMAX undulator also shows, apart from more severe effects on the orbit, a discrepancy between previous measurements and the results of the feed-forward

generation. This could indicate something like a misalignment of the undulator. If the magnetic array is notably tilted, rotated, or displaced, or a combination of the three, there would be no straight forward comparison to be made with the integrated field measurements from section 2.5.2, which are made on lines parallel to the axis. If the beam displacement measurements had been successful, it would have been possible to test this hypothesis - as it is no conclusions can be drawn.

The feed-forward generation has begun to be implemented for the coming EPU devices to be installed in the ring after the end of this project. The principles are the same, even though the EPU presents some complications. The feed-forward table needs to have two dimensions, for gap and phase, and in the case of the HIPPIE EPU, the corrector strength is dependent on the gap. An adapted algorithm has been tested in simulations, and now needs to be tested on the real machine after installation.

## 5.2 Tune and Beta-Beat

All tune measurements showed no significant impact on the tune from the undulators. Tune shifts were noticed, but these seem to be related to drift in the machine, and not the opening and closing of the undulators. The difficulties with reproducing the tune from measurement to measurement, even using the same optics, and the slight drift, also makes any eventual tune effect hard to notice. Based on design values and previous calculations, the negligible tune shift is what was expected. Similarly, no beta-beat could be seen. The asymmetrical beta functions in the ring also makes this hard to estimate.

Due to the fact that no impacts on the optics could be seen, the tune feed-forward was not implemented. Even if such a shift had been present, the lack of a reliable and non-destructive tune measurement makes the implementation difficult. New methods are under development, and a structure for the feed-forward generation has been made. Once the stronger devices are installed in the ring, these functions will be crucial.

## 5.3 Beam Displacement Measurements

Unfortunately, the beam displacement measurements proved to be severely limited. Barely a tenth of the intended range could be achieved, due to the, in this case, low strength of the correctors. Compared to other machines, MAX IV runs with very tight optics, to keep the emittance small, and this means any deviation from the intended orbit will be harder to achieve. This limitation was not expected to be so dramatic, and it is unlikely this measurement method will be usable for future devices. The scan still shows that there are no significant perturbations in the middle of the undulators, which is what was desired and expected.

## 5.4 Summary

- The effects on the beam orbit in the MAX IV 3 GeV ring has successfully been compensated for at all available gaps for the NanoMAX IVU, and for 90 % of gaps for the BioMAX IVU.
- The tune shift and beta-beat were negligible, as expected. A script for feed-forward generation for quadruples to control these effects was written, but not implemented.
- The feed-forward generation has been automatized and adapted to fit future IDs at MAX IV.
- The undulator characteristics are consistent with previous measurements and specifications; the effect of the two IVUs seem to be consistent desired values of residual integrals, etc.
- No higher order effects could be noticed within the center of the device. Other methods needs to be utilized for stronger IDs, where determining the effects on dynamic aperture, tune shift and beta-beat is crucial.

## Future Work

---

Based on the work presented in this report, a number of suggestions about future research and projects can be made.

- The feed-forward generation algorithm developed needs further adaption and testing for use on future devices with other capabilities than the IVUs.
- The feed-forward scheme for tune compensation must be developed further to be able to compensate for stronger devices.
- The difference between the two IVUs in this report could be further investigated. The larger impact of BioMAX could depend on the alignment or other unknown cause and might merit further investigation.
- Since the beam displacement measurements were so severely limited, other methods must be developed for acquiring the information which was meant to be extracted. For stronger devices, where the higher order effects are stronger, it is important to be able to locate the minimum of these effects for stable operation. They could also provide information about alignment which is currently unavailable for BioMAX and NanoMAX.

---

## References

---

- [1] R. Eriksson, ESS. [Online]. Available: <https://lu.exigus.com/file/461694>
- [2] K. Wille, *The Physics of Particle Accelerators*. Oxford University Press, 2000.
- [3] S. Mobilio, F. Boscherini, and C. Meneghini, *Synchrotron Radiation: Basics, Methods and Applications*. Springer, 2015.
- [4] R. Bartolini, John Adams Institute, Public Domain. [Online]. Available: <https://commons.wikimedia.org/w/index.php?curid=15588142>
- [5] *Strategy Plan 2013-2016 Edition 2*. MAX IV Laboratory, 2016.
- [6] H. Wiedermann, *Particle Accelerator Physics*. Springer, 2007.
- [7] A. Holzner. [Online]. Available: <https://en.wikipedia.org/w/index.php?curid=37948467>
- [8] A. Wolski and U. Liverpool, *Handbook of Accelerator Physics and Engineering*. World Scientific, 2013, ch. Dynamic Aperture.
- [9] P. Elleaume, "Insertion devices," in *CERN Accelerator School, Synchrotron Radiation and Free-Electron Lasers*, D. Brandt, Ed. CERN, 2005, pp. 83–121.
- [10] J. D. Jackson, "Classical electrodynamics." [Online]. Available: <https://commons.wikimedia.org/w/index.php?curid=15600754>
- [11] P. Schmüser, M. Dohlus, J. Rossbach, and C. Behrens, *Free-Electron Lasers in the Ultraviolet and X-Ray Regime*. Springer, 2014.
- [12] A. Ropert, "Lattices and emittances," in *CERN Accelerator School, Synchrotron Radiation and Free Electron Lasers*, S. Turner, Ed. CERN, 1998, pp. 113–126.
- [13] L. Smith, "Effects of wigglers and undulators on beam parameters," *LBL-ESG Tech*, vol. Note 24, 1986.
- [14] P. F. Tavares, S. C. Leemann, M. Sjöström, and Å. Andersson, "The MAX IV storage ring project," *Journal of Synchrotron Radiation*, vol. 21, no. 5, pp. 862–877, Sep 2014.

- 
- [15] S. Leemann, Å. Andersson, M. Eriksson, L.-J. Lindgren, E. Wallen, J. Bengtsson, and A. Streun, "Beam dynamics and expected performance of Sweden's new storage-ring light source: MAX IV," *Physical Review Special Topics - Accelerators and Beams*, vol. 12, 2009.
- [16] *Detailed Design Report MAX IV Facility*. MAX IV Laboratory, 2010.
- [17] *BioMAX – the Macromolecular Crystallography Beamline*, 2015. [Online]. Available: <https://www.maxlab.lu.se/sites/default/files/BioMAX%20Status%20November%202015.pdf>
- [18] U. Johansson, U. Vogt, and A. Mikkelsen, "NanoMAX: a hard x-ray nanoprobe beamline at MAX IV," in *Proc. SPIE*, vol. 8851, 2013.
- [19] NCEI, "Magnetic field calculators," 2016. [Online]. Available: <http://www.ngdc.noaa.gov/geomag-web/>
- [20] H. Tarawneh, private communication.
- [21] G. Portmann, J. Corbett, and A. Terebilo, "An accelerator control middle layer using Matlab," in *Proceedings of 2005 Particle Accelerator Conference*, 2005.
- [22] J. Corbett, G. Portmann, J. Safranek, and A. Terebilo, "Spear 3 commissioning software," in *Proceedings of EPAC 2004*, 2004.
- [23] A. Terebilo, "Accelerator modeling with Matlab Accelerator Toolbox," in *Proceedings of 2001 Particle Accelerator Conference*, 2001.
- [24] J. Safranek, "Experimental determination of storage ring optics using orbit response measurements," *LBL-ESG Tech*, vol. 388, 1997.
- [25] J. Safranek, G. Portmann, A. Terebilo, and C. Steier, "Matlab-based LOCO," in *Proceedings of EPAC 2002*, 2002.
- [26] E. Wallen and S. Leemann, "Strategy for neutralizing the impact of insertion devices on the MAX IV 3 GeV ring," in *Proceedings of 2011 Particle Accelerator Conference*, 2011.
- [27] S. Leemann and H. Tarawneh, "Impact of insertion devices on the MAX IV storage rings," in *Proceedings of IPAC 2015*, 2015.
- [28] J. Breunlin and Å. Andersson, "Emittance diagnostics at the MAX IV 3 GeV storage ring," in *Proceedings of IPAC 2016*, 2016.
- [29] Å. Andersson, M. Boge, A. Ludeke, V. Schlott, and A. Streun, "Determination of a small vertical electron beam profile and emittance at the Swiss Light Source." *Nuclear Instruments and Methods in Physics Research Section A: Accelerators, Spectrometers, Detectors and Associated Equipment*, vol. 591, no. 3, pp. 437 – 446, 2008.



**LUND**  
UNIVERSITY

Series of Master's theses  
Department of Electrical and Information Technology  
LU/LTH-EIT 2016-542  
<http://www.eit.lth.se>